IJFAC

Indonesian Journal of Fundamental and Applied Chemistry

Article http://ijfac.unsri.ac.id

Modification of CaO from Scallops (*Amusium Pleuronectes*) with Fe_3O_4 and SiO_2 for Adsorption of Congo Red and Methylene Blue Dye

Fera Rahma Sari[1], Widia Purwaningrum[1,2]*, Addy Rachmat[1,2]

[1] Chemistry Master's Program, Faculty of Mathematics and Natural Sciences, University of Sriwijaya, Padang Selasa Street No 524 Bukit Besar Ilir Barat I Palembang

[2] Department of Chemistry, Faculty of Mathematics and Natural Sciences, University of Sriwijaya, Jalan Palembang-Prabumulih, Indralaya, Ogan Ilir

Corresponding Author: purwaningrum@mipa.unsri.ac.id

Abstract

Congo Red and Methylene Blue dye waste from the textile industry needs to be treated before being discharged into water bodies. Adsorption is widely recognized as an effective method of contaminant removal. The use of CaO as an adsorbent has the advantages of high kinetic speed, efficient, low cost, easily accessible, and abundant. To improve the performance of CaO, it is done by compositing CaO with Fe_3O_4 and SiO_2. This study aims to synthesize a $CaO/Fe_3O_4/SiO_2$ and apply it for the adsorption of Congo red and Methylene blue dyes. The synthesis of CaO/Fe_3O_4 uses the coprecipitation method and $CaO/Fe_3O_4/SiO_2$ is synthesized using the Stober method by adding TEOS to CaO/Fe_3O_4. The results of XRD characterization show that the synthesized CaO, CaO/Fe_3O_4, and $CaO/Fe_3O_4/SiO_2$ have the same 2θ angle as the reference diffractogram data. The addition of SiO_2 was shown to prevent agglomeration, which was indicated by a decrease in the particle size of CaO/Fe_3O_4 from 70.07 to 52.42 nm in $CaO/Fe_3O_4/SiO_2$. % Adsorption efficiency for Congo Red was 86.49% Methylene Blue was 99.12%. The adsorption process of both dyes was spontaneous, following a pseudo-second-order kinetic model. Congo Red adsorption followed the Freundlich isotherm model, while Methylene Blue followed the Langmuir isotherm model.

Keywords: $CaO/Fe_3O_4/SiO_2$, adsorption, Congo red, Methylene blue

Article Info

Received 16 December 2025
Received in revised 1 February 2026
Accepted 5 February 2026
Available Online 28 February 2026

Abstrak (Indonesian)

Limbah zat warna Congo red dan metilen biru dari industri tekstil perlu diolah sebelum dibuang ke perairan. Adsorpsi diakui sebagai metode penghilangan kontaminan yang efektif. Penggunaan CaO sebagai adsorben memiliki keuntungan kinetik yang tinggi, efektif, murah, mudah diakses, dan melimpah. Peningkatkan kinerja CaO dilakukan dengan mengkompositkan CaO dengan Fe_3O_4 dan SiO_2. Penelitian ini bertujuan untuk mensintesis $CaO/Fe_3O_4/SiO_2$ dan mengaplikasikannya untuk adsorpsi zat warna Congo red dan Metilen biru. Sintesis CaO/Fe_3O_4 menngunakan metode kopresipitasi dan $CaO/Fe_3O_4/SiO_2$ disintesis menggunakan metode Stober melalui penambahan TEOS pada CaO/Fe_3O_4. Hasil karakterisasi XRD menunjukkan bahwa CaO hasil sintesis, CaO/Fe_3O_4, dan $CaO/Fe_3O_4/SiO_2$ memiliki sudut 2θ yang sama dengan data difraktogram referensi. Penambahan SiO_2 menunjukkan dapat mencegah terjadinya aglomerasi yang ditandai dengan adanya penurunan ukuran partikel CaO/Fe_3O_4 70,07 menjadi 52,42 nm pada $CaO/Fe_3O_4/SiO_2$. %Efisiensi adsorpsi untuk Congo Red 86,49% Metilen Biru 99,12%. Proses adsorpsi kedua zat warna berjalan spontan, mengikuti model kinetika pseudo orde dua. Adsorpsi Congo Red mengikuti model isotherm Freundlich sedangkan adsorpsi Metilen Biru mengikuti model isotherm Langmuir.

Kata Kunci: $CaO/Fe_3O_4/SiO_2$, adsorpsi, Congo red, Metilen biru

INTRODUCTION

The presence of dyes in wastewater originates from various industrial sectors, including the paper, textile, and printing industries [1]. In aquatic ecosystems, dyes can interfere with light penetration, slow down photosynthesis, and inhibit the development of aquatic biota [2,3]. Among the dyes frequently used are Congo red and Methylene blue. Congo red is an anionic dye classified as an aromatic compound that is toxic, carcinogenic, and difficult to decompose [4]. Methylene blue is a cationic substance widely used in various fields, such as for dyeing cotton, wool, silk, paper and for medical purposes [5-9]. Dye contaminants can be removed using adsorption methods [10,11].

CaO is a material with a structure that has a high surface area. The application of CaO as an adsorbent has advantages because it has a high kinetic speed, is effective, cheap, easily accessible, abundant, and safe for humans [3,12-14]. CaO can be the main adsorbent and is synthesized through calcination of calcium carbonate ($CaCO_3$) from various sources of eggshells, shells, fish bones and cow bones [2,3,12-20]. Scallops are an abundant source of CaO [12] which has a shell weight percentage of 75–90%. The composition of shells mostly consists of around 95% CaO, while the other components consist of organic matter and various other components [19].

Several studies have been conducted to improve the performance of CaO as an adsorbent by compositing CaO with Fe_3O_4 to form CaO/Fe_3O_4 and applying it as an adsorbent for dyes and heavy metals [3,12,13,21]. The results showed that the adsorption capacity of the CaO/Fe_3O_4 composite was greater than that of the CaO adsorbent and the separation of the adsorbent could be done using an external magnet without a filtration process. However, in its application, Fe_3O_4 can experience agglomeration. Nano-sized Fe_3O_4 has a very large surface area, making it highly unstable and prone to agglomeration. This agglomeration reduces the active surface area, which drastically reduces adsorption capacity and catalytic efficiency. Research limitations motivate the use of substances that can prevent agglomeration. The use of PDA polymers, SDS surfactants, SiO_2, alginate, etc. can protect the material from agglomeration [13,22,23].

Among oxides, SiO_2 (silica) coating is one of the most commonly used approaches for surface modification of nanoparticles, especially iron oxides such as magnetite (Fe_3O_4). This is mainly determined by the properties induced by the silica coating of Fe_3O_4 nanoparticles, such as reducing aggregation phenomena and thus increasing the stability of the resulting functional nanoparticles [24], but also improving their biocompatibility [25-27]. There are several methods that can be used for the conjugation of SiO_2 to magnetite nanoparticles. The most frequently encountered approach is the sol-gel (Stober) method, which is based on the hydrolysis of tetraethoxysilane (TEOS) in an alcoholic medium, using ammonia as a catalyst [26,27]. This method is popular due to its simplicity, but also due to the ability to obtain monodisperse coated nanoparticles, with controlled dimensions and shapes. Using this approach, the chemical composition and structure, as well as the magnetic properties of Fe_3O_4 nanoparticles, were maintained. Perez *et al*. (2018) used SiO_2 as an adsorbent for methylene blue with an adsorption capacity of 679.9 mg/g and a removal percentage of 80%, making it an excellent adsorbent for methylene blue dye [28]. Therefore, it is expected that in addition to preventing Fe_3O_4 agglomeration, SiO_2 can also improve the performance of the composite as an adsorbent.

This study developed a new CaO/Fe_3O_4/SiO_2 composite expected to have superior adsorption and separation capabilities. The composite's adsorbent capabilities were tested against anionic and cationic dyes.

MATERIALS AND METHODS

Materials

The research materials used were scallop shells, $FeCl_2{\cdot}4H_2O$, $FeCl_3{\cdot}6H_2O$, TEOS, Ethanol, ammonia, NaOH, NaCl, HCl, Congo red, Methylene blue, distilled water. All analytical quality chemicals from Merck. The instrumentation used is UV-Vis spectrophotometry, XRD, BET, SEM-EDX, VSM, FTIR, Sonicator.

Methods

Synthesis of CaO from Scallop Shell Waste (Amisium pleuronectes)

Scallop shells were thoroughly washed using distilled water, then dried in an oven at 105 °C for 3 hours. The dried scallop shells were ground and sieved using a 200-mesh sieve, then calcined at 800 °C for 6 hours [12,13].

Synthesis of CaO/Fe_3O_4 Composite

The CaO/Fe_3O_4 composite was made with a mass ratio of CaO:Fe_3O_4 = 2:1. The synthesis of the CaO/Fe_3O_4 composite was carried out in the same way as the Fe_3O_4 synthesis method by mixing $FeCl_3{\cdot}6H_2O$ (4.66 g) and $FeCl_2{\cdot}4H_2O$ (1.718 g) then dissolving it in 50 mL of deionized water and adding 4 g of CaO [12].

Synthesis of $Fe_3O_4/SiO_2/CaO$ Composite

The Stober method, adapted from Hariani et al., [29], is used for the synthesis of $CaO/Fe_3O_4/SiO_2$. $CaO/Fe_3O_4/SiO_2$ synthesis was carried out by dissolving 0.2 g of CaO/Fe_3O_4 in 50 mL of ethanol, 10 mL of distilled water, and 1.2 mL of ammonia solution one hour. Then, 20 mL of a solution made from 2 mL of TEOS diluted in 20 mL of ethanol was slowly added. The sonication process was then maintained for approximately one hour. The precipitate was separated from the solution using an external magnet. Next, the precipitate underwent a thorough washing process involving distilled water and ethanol. Finally, the precipitate was dried under vacuum at 60 °C.

Material Characterization

The obtained materials (CaO/Fe_3O_4 and $CaO/Fe_3O_4/SiO_2$) were characterized using XRD to determine the phase type, BET to determine the surface area, pore volume, and pore diameter, SEM-EDX to determine the morphology and elemental composition, VSM to determine the magnetic properties and FTIR to identify the functional groups. The pH of the $CaO/Fe_3O_4/SiO_2$ composites was determined using NaCl solution as the electrolyte, and NaOH and HCl to adjust the pH of the solution [30].

Determination of Optimum Adsorption Conditions

The optimum adsorption conditions for the $CaO/Fe_3O_4/SiO_2$ composite on Congo Red and Methylene Blue dyes were determined at contact times of 15, 30, 45, 60, 75, and 90 minutes; various concentrations of Congo Red (5, 10, 15, 20, and 25 mg/L) and Methylene Blue (5, 10, 15, 20, 25, 30, 35, 40, 45, and 50 mg/L); and various adsorbent weights of 0.01; 0.05; 0.1; 0.15; 0.2; and 0.25 g; and temperatures of 25, 30, 35, 45, and 50°C.

Data Analysis

Determination of Adsorption Kinetics

Adsorption kinetics studies are important to conduct, as they will provide valuable information about the reaction pathway and control mechanisms of the adsorption process. Kinetic studies were conducted to investigate the adsorption kinetics, pseudo-first-order and pseudo-second-order kinetic models. The pseudo- first-order kinetics for the adsorption process is described by equation (1):

$$\log (Q_e - Q_t) = \log Q_e - \frac{k_1}{2{,}303} t \quad \text{.....(1)}$$

where Qt is the amount of adsorbate adsorbed at time t (mg/g), Qe is the equilibrium adsorption capacity (mg/g), t is the time in minutes, and K1 is the first-order rate constant. The linear form of the pseudo-second-order kinetic model is expressed through equation (2):

$$\frac{t}{Q_t} = \frac{1}{K_2 Q_e^2} + \frac{t}{Q_e} \quad \text{.....(2)}$$

where Qt is the amount of adsorbate adsorbed at time t (mg/g), Qe is the equilibrium adsorption capacity (mg/g), t is the time in minutes, and K_2 is the second-order rate constant [30-32].

Determination of Adsorption Isotherms

The Langmuir isotherm defines that the maximum adsorbent capacity occurs due to the presence of a single layer (monolayer) of adsorbate on the surface of the adsorbent. The Langmuir isotherm model is represented in equation (3):

$$\frac{C_e}{Q_e} = \frac{1}{Q_m} C_e + \frac{1}{Q_m K_L} \quad \text{.....(3)}$$

where Ce (mg L--1) is the concentration of solute in the solution after adsorption equilibrium occurs, Qe (mg g-1) is the amount of substance adsorbed per gram of adsorbent, Qm (mg g-1) is the maximum adsorption capacity and KL is the Langmuir adsorption constant. The Freundlich equation is shown in equation (4).

$$\log Q_e = \log K_F + \frac{1}{n} \log C_e \quad \text{.....(4)}$$

where K_F (mg L^1) is the adsorption capacity and n is the adsorption intensity. Langmuir isotherm, K_L can be calculated from the intercept of the graph of the relationship between Ce/Qe and Ce, while Qm is calculated from the slope of the graph. Freundlich isotherm, K_F can be calculated from the intercept of the graph of the relationship between log Qe and log Ce, while n is calculated from the slope of the graph [33-35].

Determination of Adsorption Thermodynamics

Thermodynamics are studied from temperature variation during adsorption. Thermodynamic parameters of adsorption include ΔG^o, ΔS^o and ΔH^o which can be calculated using Ce and Qe data from temperature variations. Determination of adsorption thermodynamics is done by making a curve between 1/T vs ln (Qe/Ce). The regression equation obtained shows a slope of - $\Delta H/RT$ and an intercept of $\Delta S/R$, so that the values of ΔH and ΔS can be calculated from the slope and intercept [36].

RESULTS AND DISCUSSION

Synthesized Materials

The materials synthesized in this study were CaO, CaO/Fe_3O_4, and $CaO/Fe_3O_4/SiO_2$. CaO was obtained

by calcining scallop shells at 800 °C for 6 hours. The reaction follows equation (5).

$$CaCO_3\ (p) \rightarrow CaO\ (p) + CO_2\ (g) \quad (5)$$

The synthesized CaO was used for the synthesis of CaO/Fe_3O_4 using the coprecipitation method, where CaO was added to the Fe^{3+} solution and Fe^{2+} solution before adding the NaOH solution. The reaction that occurred, according to equation 6.

$$CaO_{(S)} + Fe^{2+}_{(aq)} + 2Fe^{3+}_{(aq)} + 8OH^-_{(aq)} \rightarrow CaO/Fe_3O_{4(s)} + 4H_2O_{(l)} \quad (6)$$

The synthesized CaO/Fe_3O_4 was then used to synthesize $CaO/Fe_3O_4/SiO_2$ using the Stober method with the addition of TEOS as a precursor to SiO_2 according to reaction (7,8).

$$Si(OC_2H_5)_4 + 4H_2O \rightarrow Si(OH)_4 + 4C_2H_5OH \quad (7)$$

$$Si(OH)_4 + 4C_2H_5OH + CaO/Fe_3O_4 \rightarrow CaO/Fe_3O_4/SiO_2 + 2H_2O \quad (8)$$

TEOS hydrolyzes in alkaline conditions (using ammonia/NH_4OH) to produce silanols and ethanol. Silanol molecules bond with each other through a condensation process to form a silica (SiO_2) network that coats the Fe_3O_4 core in the CaO/Fe_3O_4 composite

XRD Characterization Results

XRD characterization aims to obtain the 2θ angle position, peak intensity and crystal phase obtained from the synthesis results. The results of the XRD characterization of CaO, CaO/Fe_3O_4, $CaO/Fe_3O_4/SiO_2$ synthesis results were compared with data from the Joint Committee on Powder Diffraction Standards (JCPDS) No. 82-1690 [12,13] for CaO, JCPDS No. 65-3107 [12,13] for Fe_3O_4, JCPDS No. 29–0085 [37] for SiO_2. **Figure** 4 shows the diffraction pattern of CaO, CaO/Fe_3O_4, $CaO/Fe_3O_4/SiO_2$. **Figure** 1 shows diffraction pattern of CaO, CaO/Fe_3O_4, $CaO/Fe_3O_4/SiO_2$.

SEM Characterization Results

SEM characterization aims to observe the surface morphology of the composite. Materials with small particle sizes such as nano-sized Fe3O4 in the CaO/Fe3O4 composite tend to aggregate to reduce surface energy. In addition, the occurrence of Van der Waals forces causes the particles to attract each other [38]. The SEM characterization results show that there are differences in surface morphology in the $CaO/Fe_3O_4/SiO_2$ composite and the CaO/Fe_3O_4 composite. **Figure** 2 shows that at 500x or 1000x magnification, the $CaO/Fe_3O_4/SiO_2$ composite has a smaller particle morphology compared to the CaO/Fe_3O_4 composite. This indicates that the addition of SiO_2 to the CaO/Fe_3O_4 composite successfully reduces the agglomeration that occurs in the CaO/Fe_3O_4 composite caused by the ease of Fe_3O_4 agglomeration. This data corresponds to the particle size value of the $CaO/Fe_3O_4/SiO_2$ composite (52.42 nm) which is smaller than the CaO/Fe_3O_4 composite (70.70 nm) obtained from the calculation results of the 2θ angle using the Debye Scherer formula (**Table** 1).

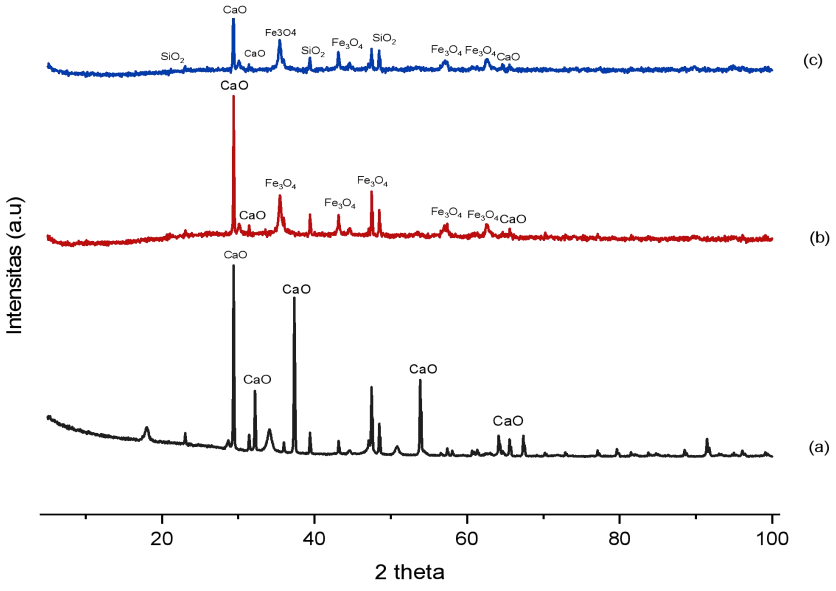

Figure1. Diffraction pattern of CaO, CaO/Fe_3O_4, $CaO/Fe_3O_4/SiO_2$.

Table 1. JCPDS reference and research material 2θ angle and crystallite size

JCPDS	Material	Sudut 2θ	Crystal Size (nm)
No. 82-1690	CaO	32.59°, 37.75°, 53.54°, 64.10°, 67.76°	-
No. 65-3107	Fe_3O_4	30.15°, 35.52°, 43.32°, 47.27°, 53.71°, 57.21°, 62.94	-
No. 29–0085	SiO_2	20.8°, 26.6°, 36.5°, 39.5°, 50.1°, 59.9°	-
-	CaO	17,89°, 23,11°, 28,65°, 29,39°, 31,46°, 32,18°, 33,97°, 36,04°, 37,34°, 39,38°, 43,14°, 44,62°, 47,46°, 48,49°, 50,83°, 53,83°, 57,40°, 58,00°, 64,13°, 65,55°, 67,36°	56.90
-	CaO/Fe_3O_4	23,08°, 29,40°, 30,20°, 31,42°, 35,45°, 39,38°, 43,14°, 44,66°, 47,46°, 48,49°, 57,40°, 62,54°, 65,58°, 70,23°, 77,10°	70.70
-	$CaO/Fe_3O_4/SiO_2$	21,16°, 23,04°, 29,36°, 30,07°, 31,39°, 35,42°, 39,38°, 43,11°, 47,46°, 48,45°, 57,10°, 62,58°, 64,52°, 65,55°	52.42

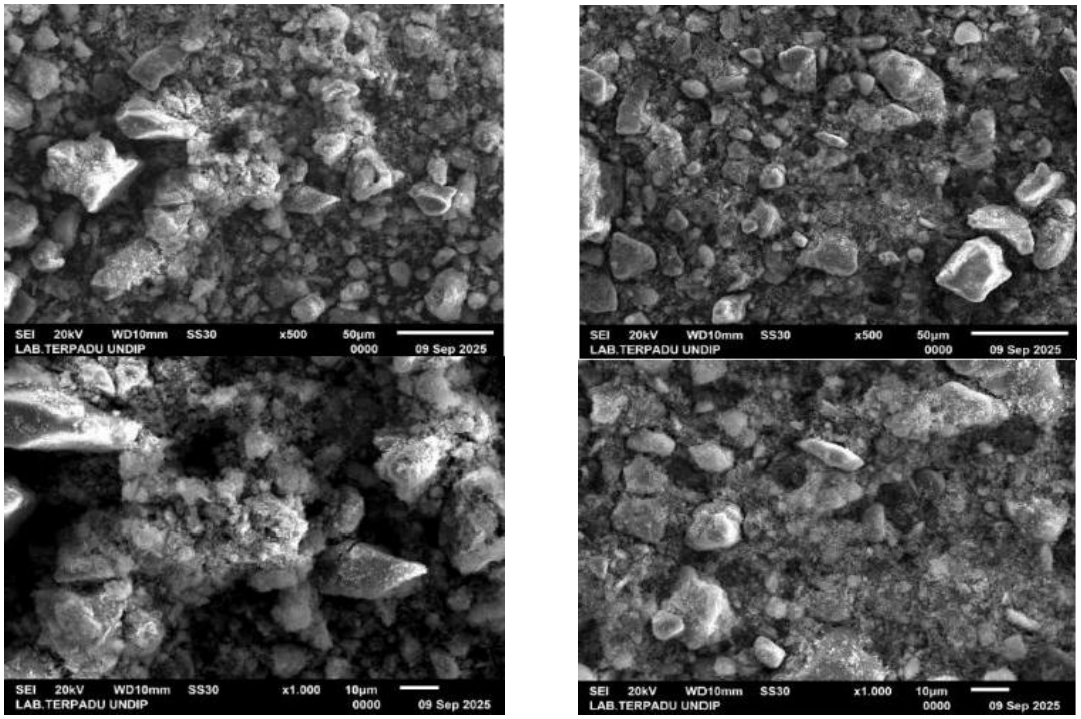

Figure 2. SEM with 500× and 1000× magnification: CaO/Fe_3O_4 (left) and $CaO/Fe_3O_4/SiO_2$ (right)

BET Characterization Results

The BET analysis results showed that the specific surface area of the CaO/Fe_3O_4 composite was 61.6355 m^2/g, while that of $CaO/Fe_3O_4/SiO_2$ was 34.9289 m^2/g. The pore volume of each composite was 0.204899 cm^3/g and 0.127543 cm^3/g, respectively. The decrease in surface area and pore volume in the composite with the addition of SiO_2 indicates that the silica phase from TEOS fills and covers some of the pores of the material. This phenomenon is common in $Fe_3O_4@SiO_2$ materials, where silica acts as a supporting matrix that increases structural stability but can reduce the specific surface area [42].

The average pore diameter based on the BJH method for CaO/Fe_3O_4 is 15.372 nm and for $CaO/Fe_3O_4/SiO_2$ is 13.866 nm. This value indicates that both composites are classified as mesoporous materials based on the IUPAC classification (2–50 nm). The mesoporous structure is very advantageous for adsorbent applications because it can facilitate the

diffusion of adsorbate molecules into the pores effectively [42]. From **Table** 2, it can be seen that the surface area of the $CaO/Fe_3O_4/SiO_2$ composite decreased compared to the CaO/Fe_3O_4 composite due to the presence of SiO_2 occupying the CaO pores, so that the pore volume decreased.

The decrease in specific surface area and pore volume after silica coating is a common phenomenon, where the silica layer tends to cover small pores (micropores) or clog mesoporous pores in the base material. Despite the reduced surface area, adsorption efficiency often remains high or even increases. Based on the principles of material chemistry, this occurs due to several main factors, namely an increased number of active functional groups (Si-OH). The SiO_2 coating introduces abundant silanol groups (-OH) on the surface. These groups serve as highly effective active sites for binding adsorbates through hydrogen bonding or ion exchange. Another factor is active site accessibility. Small pores covered by silica may initially be inaccessible to adsorbate molecules. Structured silica coatings can create more "open" and accessible active sites on the outer surface (surface chemistry modification), making the entire active surface more efficient at binding substances.

Table 2. BET characterization of CaO/Fe_3O_4 and $CaO/Fe_3O_4/SiO_2$

Composite	BET Surface area (m^2/g)	Pore volume (cm^3/g)	Adsorpstion Average pore diameter (nm)	Desorption Average pore diameter (nm)	BJH Average pore diameter (nm)
CaO/Fe_3O_4	61,6355	0,204899	14,606	9,025	15,372
$CaO/Fe_3O_4/SiO_2$	34,9289	0,127543	13,297	8,370	13,866

VSM Characterization Results

The VSM characterization results showed that the magnetic saturation value of the CaO/Fe_3O_4 composite was greater than that of the $CaO/Fe_3O_4/SiO_2$ composite, namely 57.499 emu/g and 46.928 emu/g, respectively, as shown in **Figure** 3. This can be explained by the higher percentage of Fe_3O_4 in the CaO/Fe_3O_4 composite than in the $CaO/Fe_3O_4/SiO_2$ composite. Hu et al. reported that the saturation magnetization of Fe_3O_4 was 75.3 emu g^{-1} [39]. The results of this study are consistent with research conducted by Hariani *et al*. [40]. In general, compositing, including coating materials, tends to reduce magnetic properties, as confirmed by Wei *et al*. [41].

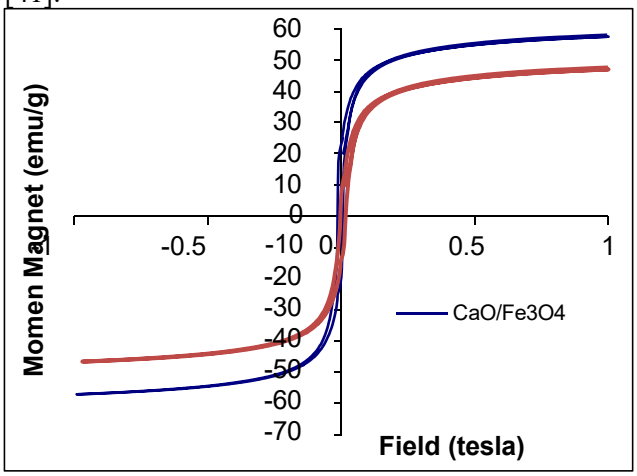

Figure 3. Graph of magnetic saturation values of CaO/Fe_3O_4 and $CaO/Fe_3O_4/SiO_2$

Results of pH Point Zero Charge (pHpzc) Determination on $CaO/Fe_3O_4/SiO_2$ Composite

Determination of pHpzc (pH Point of Zero Charge) was performed to determine the neutral pH of the adsorbent. This value was obtained by crossing the initial and final pH curves for the $CaO/Fe_3O_4/SiO_2$ adsorbent, as depicted in **Figure** 4.

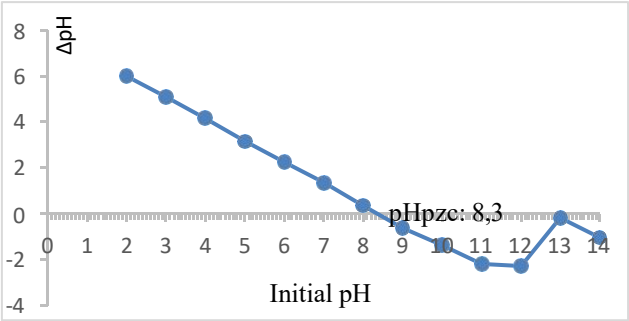

Figure 4. pHpzc graph of the synthesized $CaO/Fe_3O_4/SiO_2$ composite

In **Figure** 4, the pHpzc value of the $CaO/Fe_3O_4/SiO_2$ composite is set at 8.3. This value indicates that the composite surface is positively charged when the pH is below 8.3, while at a pH above this value the composite surface tends to be negatively charged [12,13,17]. Congo red, which is an anionic dye, has a solution pH of 6.1. Therefore, the electrostatic interaction between the positive charge of the composite and the negative charge of Congo red will maximize the adsorption process when the pH is below 8.3. This condition is in accordance with

the pH of the Congo red solution, which is 6.1 so that adsorption can occur optimally without the need for adjustments to the solution pH. Methylene blue is a cationic dye that is positively charged, so the adsorption mechanism is more effective if the composite surface is negatively charged. This can be achieved under alkaline pH conditions, namely when the solution pH is adjusted higher than the pHpzc value. pH regulation is an important factor in increasing the effectiveness of methylene blue adsorption on $CaO/Fe_3O_4/SiO_2$ composites, the methylene blue adsorption process is carried out at pH 12 [17].

Determining Optimum Conditions for Congo Red and Methylene Blue Adsorption

Optimum adsorption conditions were determined by varying the contact time, dye concentration, adsorbent weight, and temperature. The effect of each independent variable on the adsorption efficiency percentage was observed. The results of the study on the effect of each variable on Congo red and methylene blue dye percentage efficiency are shown in **Figure** 5- 8.

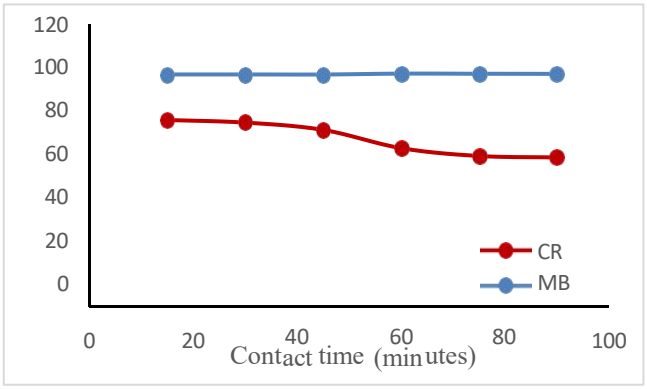

Figure 5. The effect of contact time on % efficiency

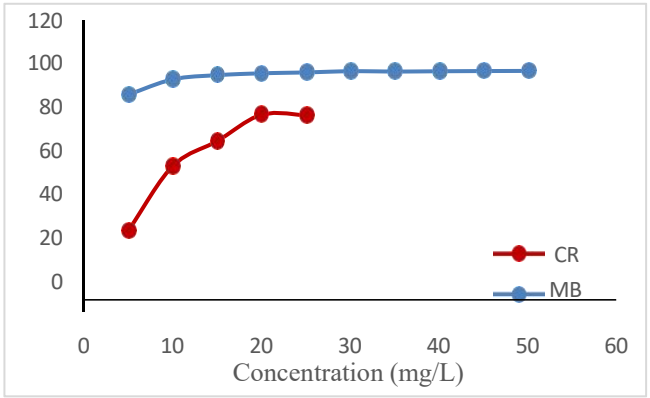

Figure 6. The effect of concentration on % efficiency

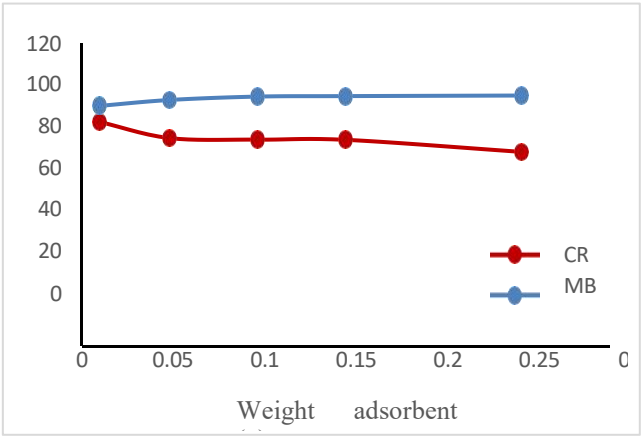

Figure 7. The effect of adsorbent weight on % efficiency

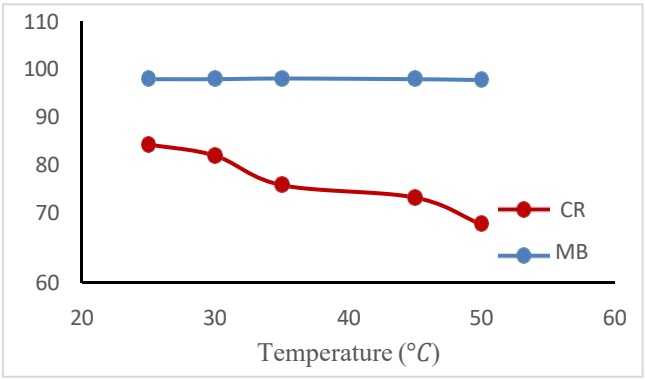

Figure 8. The effect of temperature on % efficiency

The results of the study showed that the optimum conditions for adsorption of the $CaO/Fe_3O_4/SiO_2$ composite on Congo red dye were different from the optimum conditions for adsorption of the $CaO/Fe_3O_4/SiO_2$ composite on Methylene blue dye. This is because the Congo red dye has a different structure, molecular weight and charge than the Methylene Blue dye. The optimum conditions for adsorption of the Congo red dye were at a contact time of 15 minutes, a concentration of 20 ppm, an adsorbent weight of 0.01 g and a temperature of 25 °C with an efficiency of 86.49%. The optimum conditions for adsorption of the Methylene blue dye were at a contact time of 60 minutes, a concentration of 50 ppm, an adsorbent weight of 0.25 g and a temperature of 35 °C with an efficiency of 99.12%.

The molecular weight of Congo Red is about 696.7 g/mol, with the molecular formula being $C_{32}H_{22}N_6Na_2O_6S_2$, while Methylene blue has a molecular weight of about 319.85 g/mol with the molecular formula being $C_{16}H_{18}ClN_3S$. Congo red has a much larger size than Methylene blue. Large molecules may have complex spatial conformations that not only limit access to the pores, but also take up more space on the adsorbent surface, thereby reducing

the total number of molecules that can adhere in a single layer (monolayer). The ability of an adsorbate to reach the active sites of an adsorbent depends heavily on its molecular size. Low-molecular-weight molecules have greater mobility and readily diffuse into deeper pores, while high-molecular-weight molecules are inhibited.

Congo red is an anionic dye so that at the initial pH Congo red has a stronger interaction with the $CaO/Fe_3O_4/SiO_2$ composite compared to Methylene blue dye. However, the results of the study showed that the %efficiency of Methylene blue was greater than Congo red, this indicates that the influence of molecular size is more dominant in the adsorption process between the $CaO/Fe_3O_4/SiO_2$ composite and the dye compared to the ion-ion interaction between the $CaO/Fe_3O_4/SiO_2$ composite and the dye. The final results of the adsorption of Congo red and Methylene blue dyes using the $CaO/Fe_3O_4/SiO_2$ composite can be seen in **Figure** 9. Sufficient contact time allows the adsorbent to absorb as much adsorbate as possible. After reaching the optimum time (saturation time), the pores of the adsorbent are full, and additional time can cause desorption (re-release of the adsorbate), reducing efficiency [43]. The optimum adsorption conditions are shown in **Table** 3.

Figure 9. Adsorption of Congo red and methylene blue dyes

Adsorption Kinetic of Dyes

The purpose of determining an adsorption kinetic model is to understand the rate of the adsorption process, identify the adsorption mechanism, evaluate the performance of the adsorbent, determine the time required to reach equilibrium, and obtain kinetic parameters (such as rate constants) for optimizing waste treatment applications. This model helps predict how the adsorbent will interact with the adsorbate over time. Kinetic models such as pseudo-first-order and pseudo-second-order help determine whether the adsorption rate is limited by diffusion (particle movement) or chemical interactions at the adsorbent surface.

Table 3. The optimum adsorption conditions of dyes

Dyes	Optimum adsorption conditions				Efficiency
	Contact time	Concentration	Weight adsorben	Temperature	
Congo red	15	20 mg/L	0.1 g	25ºC	86.49 %
Methylene blue	60	50 mg /L	0.1 g	35ºC	99.12 %

Table 4. Kinetic model of dyes

Kinetics Model	Parameter	Congo red	Methylene blue
Pseudo first order	R^2	0.614	0.707
	K1	0.040	0.052
	qe.calc	8.824	0.211
Pseudo second order	R^2	0.993	0.999
	K2	0.050	0.637
	qe.calc	2.876	5.030
	qe.exp	3.358	5.058

Adsorption kinetic model can provide an overview of the evaluation of adsorbent performance, namely how quickly a material (adsorbent) can remove pollutants (adsorbate), which is important for practical applications such as water purification. The adsorption kinetic model is used to determine the equilibrium time, namely to predict how long the contact time is needed between the adsorbent and adsorbate for the adsorption process to reach saturation (equilibrium) [44-46].

The results of the study showed that the adsorption kinetics of the $CaO/Fe_3O_4/SiO_2$ composite on Congo red and Methylene blue dyes followed a pseudo-second-order kinetics model, as shown in Table 4. The pseudo-second-order kinetics model is a model that explains the rate of adsorption of substances where the rate-limiting step is the chemical interaction (chemisorption) between the adsorbate and the adsorbent, not just the physical process, and this rate depends on the adsorption capacity or the number of active sites on the adsorbent surface, not just the adsorbate concentration. This shows that the adsorption that occurs between the $CaO/Fe_3O_4/SiO_2$ composite with Congo red and Methylene blue dyes

involves chemical bonds or electron exchange (chemisorption). The adsorption rate depends on the number of active sites available on the adsorbent surface and the adsorbate concentration at equilibrium time (qe) [47,48].

Adsorption Isotherm of Dyes

The adsorption isotherm model is used to understand the mechanism, capacity, and equilibrium characteristics of the adsorption process of a substance (adsorbate) onto the adsorbent surface at a constant temperature, which is very important for evaluating adsorbent performance and designing industrial adsorption systems (such as water treatment). This model helps predict how much substance can be adsorbed and its physical interactions (physical/chemical, mono/multi-layer) [49,50]. By knowing the adsorption isotherm model, the adsorption mechanism can be known whether the adsorption is physical (van der Waals force, multi-layer) or chemical (formation of chemical bonds, mono-layer). In addition, determining the adsorption isotherm model can be used to determine the maximum capacity (Qm), by calculating the maximum amount of adsorbate that can be accommodated by the adsorbent [34,35].

Tabel 5. Adsorption isotherm model of dyes

Isotherm Model	Parameter	Congo red	Methylene blue
Langmuir	R^2	0.361	0.859
	KL	0,250	2,506
	qm	0.197	0.236
Freundlich	R^2	0.898	0.632
	KF	0.294	0.009
	n	4.000	0.133

The adsorption of $CaO/Fe_3O_4/SiO_2$ composite on Congo red dye follows the Freundlich adsorption isotherm model, while on Methylene blue dye it follows the Langmuir adsorption isotherm model (**Table** 5). This shows that the adsorption of Methylene blue dye is assumed to occur in a monolayer and homogeneous adsorption, suitable for chemical adsorption, while the adsorption of Congo red dye is assumed to occur in a multilayer or inhomogeneous surface adsorption. **Table** 6 shows the adsorption capacity of various adsorbents that have been used to adsorb Congo red and Methylene blue.

Table 6. Comparison of adsorption capacity of various adsorbents

Adsorbent	Dyes	
	Congo Red	Methylene blue
	Adsorption capacity (mg/g)	Adsorption capacity (mg/g)
Graphene/magnetite [51]		43.82
DNPH-γ-alumina [52]		32.8
Chaff [53]		20.3
Silkworm exuviae [54]		25.5
Poly (vinyl alcohol) [55]		13.80
Lava [56]		10.32
CaO [17]		34.48
CaO/SDS [17		56.82
CaO/Fe_3O_4 [3]	45,16	
MgO-bentonite clay nanocomposites [57]	11.2	
Waste wood biomass [58]	8	
Sawdust [59]]	2.86	
Eichormia crassipes biomass [60]	14.49	
Raw chestnut peels [61]	4.32	
Parkia biglobosa sawdust [62]	21.65	
Sargassum latifolium [63]	20.97	
Spathodea campanulate leaves [64]	12.67	
$CaO/Fe_3O_4/SiO_2$ (This study)	3.47	9.81

Thermodynamic Quantities of Dyes

The main purpose of determining thermodynamic quantities (such as Gibbs free energy, enthalpy, and entropy) in the adsorption process is to understand the feasibility (spontaneity) and the mechanism of interaction between the adsorbent

(absorbent material) and the adsorbate (absorbed substance). The value of the standard Gibbs free energy change (ΔG°) indicates whether the adsorption process will occur spontaneously or not. The standard enthalpy change (ΔH°) provides information about the nature of the energy or heat involved in the process. The standard entropy change (ΔS°) measures the level of disorder or randomness in the system during adsorption [65]. The graph of the relationship between 1/T and ln (Qe/Ce) of the $CaO/Fe_3O_4/SiO_2$ composite against dye is shown in **Figures** 10 and 11.

Table 7 shows that the adsorption process of Congo red dye has a ΔH° of -20.21 kJ/mol, ΔS° of -0.066 J/K mol and ΔG° negative value up to a temperature of 30 °C and positive value above 30 °C. While the adsorption process of Methylene blue dye has a ΔH° of -2.92 kJ/mol, ΔS° of 0.01 J/K mol and ΔG° negative value at all temperature variations up to a temperature of 55 °C. This shows that the adsorption process of the two dyes is exothermic and occurs spontaneously.

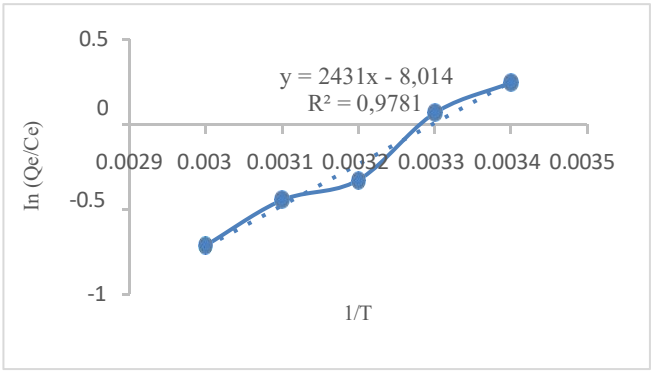

Figure 10. Plot of 1/T and ln (Qe/Ce) of $CaO/Fe_3O_4/SiO_2$ toward Congo red

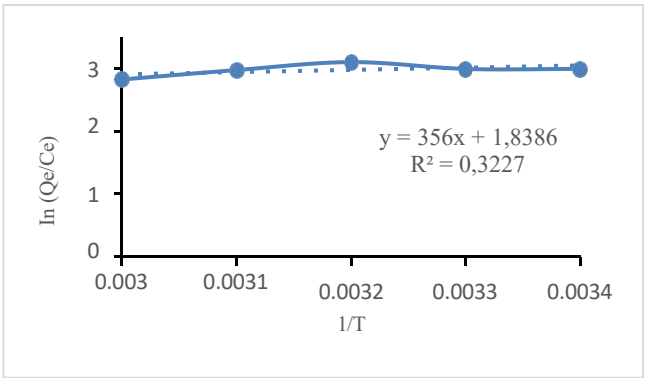

Figure 11. Plot of 1/T and ln (Qe/Ce) of $CaO/Fe_3O_4/SiO_2$ composites against Methylene blue

The adsorption process generally involves the movement of molecules from the liquid/gas phase to the solid surface, which usually results in a decrease in entropy (negative ΔS° value) due to increased order.

Tabel 7. Thermodynamic parameters for the adsorption process of Congo Red and Methylene Blue

T (K)	Congo red			Methylene blu		
	ΔH⁰ (J mol⁻¹)	ΔS⁰ (JK⁻¹mol⁻¹)	ΔG⁰ (J mol⁻¹)	ΔH⁰ (J mol⁻¹)	ΔS⁰ (JK⁻¹mol⁻¹)	ΔG⁰ (J mol⁻¹)
298	-	-	-0,55	-	-	-5,90
303	-	-	-0,23	-	-	-5,95
308	-20,21	-0,066	0,11	-2,92	0,01	-6,00
318	-	-	0,77	-	-	--6,10
323	-	-	1,10	-	-	-6,15

FTIR Characterization Results

FTIR analysis was performed to identify the functional groups present in the $CaO/Fe_3O_4/SiO_2$ composite before and after the adsorption process. This analysis aimed to demonstrate the successful synthesis of the $CaO/Fe_3O_4/SiO_2$ composite and the adsorption of Congo red and methylene blue dyes by the $CaO/Fe_3O_4/SiO_2$ composite. The FTIR spectra, adsorption area and bond type of the $CaO/Fe_3O_4/SiO_2$ composite before and after the adsorption process are shown in **Figure** 12 and **Table** 8.

The FTIR spectra of the $CaO/Fe_3O_4/SiO_2$ composite show the presence of Ca-O bonds in the absorption region of 875.68 cm-1, Fe-O functional bonds at wave numbers of 576.72 cm-1 [3,12,13,52] and indicate the presence of Si-O-Si functional groups at wave numbers of 1087.85 cm-1 [66,67]. In addition, there is also a Ca- OH functional group at 1431.18 cm-1 indicating that CaO has undergone hydration or reacted with water to form calcium hydroxide ($Ca(OH)_2$). The presence of O-H (hydroxyl) functional groups in the wave number region of 3425.58 cm-1 in the FTIR spectrum of $CaO/Fe_3O_4/SiO_2$ composites generally indicates the formation of silanol groups (Si-OH) (3400-3500 cm-1), adsorption of water by CaO with a broad peak in the region of 3400-3600 cm^{-1} or groups originating from $Ca(OH)_2$ which occurs because CaO tends to react with air humidity [3,12,13,52,53].

FTIR analysis of $CaO/Fe_3O_4/SiO_2$ composite after adsorption of Congo red dye, did not show any increase in spectrum so it can be concluded that Congo red absorption was not detected due to the small concentration of Congo red absorbed. FTIR analysis of $CaO/Fe_3O_4/SiO_2$ composite after adsorption of Methylene blue dye showed an absorption peak at wave number 2873.94 cm^{-1}. This indicates the presence

of C-H (aliphatic) functional groups from Methylene blue.

Tabel 8. Adsorption area and bond type in $CaO/Fe_3O_4/SiO_2$ composite before and after adsorption

Material	Fe-O (cm^{-1})	Ca-O (cm^{-1})	Ca-OH (cm^{-1})	OH (cm^{-1})	Si-O-Si (cm^{-1})	C-H (cm^{-1})
$CaO/Fe_3O_4/SiO_2$	576.72	875.68	1431.18	3425.58	1087.85	-
$CaO/Fe_3O_4/SiO_2$ - CR	574.79	875.68	1427.32	3425.58	1087.85	-
$CaO/Fe_3O_4/SiO_2$- MB	572.86	875.68	1431.18	3402.43	1087.85	2873.94

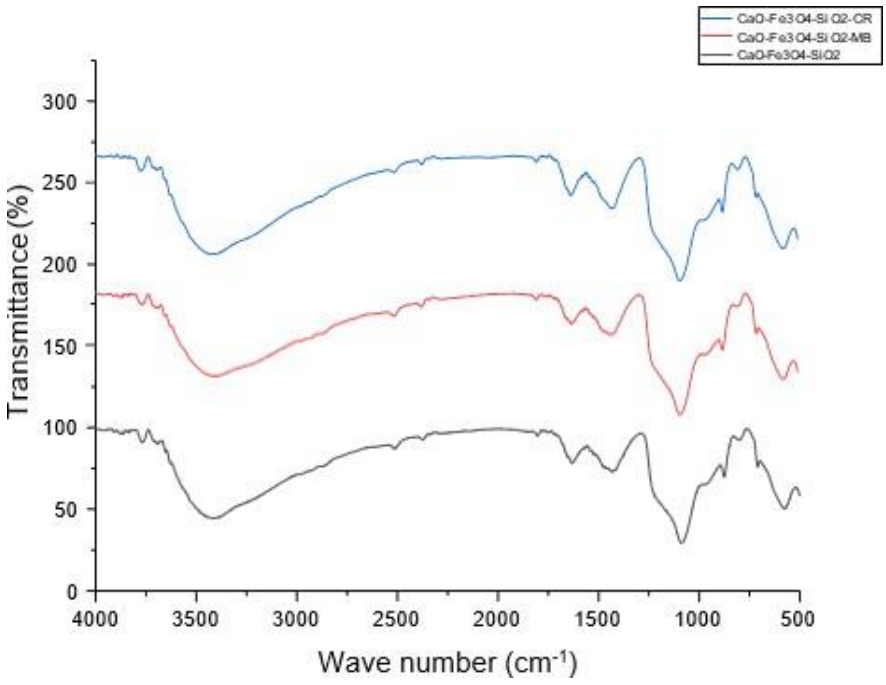

Figure 12. FTIR Spectrum of $CaO/Fe_3O_4/SiO_2$ before and after adsorption

CONCLUSION

The $CaO/Fe_3O_4/SiO_2$ composite was successfully synthesized. The addition of SiO_2 successfully reduces the particle size by 25.86%. The adsorption efficiency percentages for Congo Red and Methylene Blue dyes were 86.49% and 99.12%, respectively. The adsorption process was spontaneous, followed a pseudo-second-order kinetic model. The adsorption of Congo Red followed the Freundlich isotherm model. The adsorption of Methylene Blue followed the Langmuir isotherm model.

ACKNOWLEDGMENT

The research was funded by the Directorate General of Research and Development, Ministry of Higher Education, Science and Technology, for the 2025 fiscal year based on Decree No. 0419/C3/DT.05.00/2025 with Contract Number 109/C3/DT.05.00/PL/2025.

REFERENCES

[1] H. Lee, S. Fiore, & F. Berruti, "Biomass and bioenergy adsorption of methyl orange and methylene blue on activated biocarbon derived from birchwood pellets." *Biomass and bioenergy*, *Biomass and Bioenergy,* Vol. 191, p. 107446, Dec 2024..

[2] E. Misran, M.D. Supardan, D.A. Iryani, V. Pramananda, A.F. Sihombing, & D.V. Sitorus, "Ultrasonic assisted adsorption of methylene blue using blood clam shell as a low-cost adsorbent." *Results in engineering*, vol. 23, 2024.

[3] W. Purwaningrum, F. Riyanti, J. Julinar, P.L.

Hariani, B.R. Ahadito, S. Chodijah, & V.P. Safira, "Synthesis and characterization of nanoparticle composite CaO/Fe_3O_4 from duck egg shells and its application for congo red and procion red MX-5b dyes adsorption." *Indonesian Journal of Fundamental and Applied Chemistry*, vol. 9, no. 2, pp. 103–110, 2024.

[4] S. Chatterjee, N. Guha, S. Krishnan, A.K. Singh, P. Mathur, & D.K. Rai, "Selective and Recyclable Congo Red Dye Adsorption by Spherical Fe_3O_4 Nanoparticles Functionalized with 1,2,4,5-Benzenetetracarboxylic Acid," *Scientific Reports*, vol. 10, pp. 111, 2020.

[5] A. Siciliano, G.M. Curcio, C. Limonti, S. Masi, & M. Greco, "Methylene Blue Adsorption on Thermo Plasma Expanded Graphite in A Multilayer Column System." *Journal of Environmental Management*, vol. 296, July 2021.

[6] M.H. Calimli, M.S. Nas, H. Buran, S.D. Mustafov, O. Demirbas, F. Sen, "Preparation, characterization and adsorption kinetics of methylene blue dye in reduced-graphene oxide supported nanoadsorbents." *Journal of Molecular Liquids*, vol. 309, 2020.

[7] S. Liu, H. Ge, C. Wang, Y. Zou, J. Liu, "Agricultural waste/graphene oxide 3D bio-adsorbent for highly efficient removal of methylene blue from water pollution." *Science of the Total Environment*, vol. 628, pp. 959–968, 2018.

[8] A.A. Al-Massaedha, F.I. Khalilib, A. Al Shra'aha, "Adsorptive removal of cationic dyes (methylene blue and crystal violet) from aqueous solutions using anionic polyacrylamide-based monolith," *Desalination and Water Treatment*, vol. 270, pp. 260–274, 2020.

[9] F. Meng, J. Zhang, Q. Liu, D. Wang, F. Li, & J. Wang, "Biochar derived from biogas fermentation residue with enhanced absorption property suitable for efficient absorption of methylene blue in aqueous." *Colloids and surfaces A: Physicochemical and Engineering Aspects*, vol. 703, 2024.

[10] J. Miao, X. Zhao, Y.X. Zhang, Z.L. Lei, & Z.H. Liu, "Preparation of hollow hierarchical porous CoMgAl-borate LDH ball-flower and its calcinated product with extraordinary adsorption capacity for congo red and methyl orange." *Applied Clay Science*, vol. 207, 2021.

[11] S. Hegazy, N.A. Abdelwahab, A.M. Ramadan, & S.K. Mohamed, "Magnetic Fe_3O_4-grafted cellulose/graphene oxide nanocomposite for methylene blue removal from aqueous solutions: Synthesis and characterization. *Next Materials*, vol. 3, 2024.

[12] W. Purwaningrum, H. Hasanudin, A. Rachmat, F. Riyanti, P.L. Hariani, "Modification of Calcium Oxide from Green Mussel Shell with Iron Oxide as a Potential Adsorbent for the Removal of Iron and Manganese Ions from Acid Mine Drainage." *Journal of Ecological Engineering*, vol. 23, no. 11, pp. 188–201, 2022.

[13] W. Purwaningrum, H. Hasanudin, A. Rachmat, F. Riyanti, P.L. Hariani, "Magnetic Composite for Efficient Adsorption of Iron and Manganese Ions from Aqueous Solution." *Ecological Engineering & Environmental Technology*, vol. 24, no. 8, pp. 143–154, 2023.

[14] S. Thakur, S. Singh, & B. Pal, "Superior adsorption removal of dye and high catalytic activity for transesterification reaction displayed by crystalline CaO nanocubes extracted from mollusc shells," *Fuel Processing Technology*, vol. 213, 2021.

[15] A.A. Ayodeji, I.E. Blessing, F.O. Sunday, "Data on calcium oxide and cow bone catalysts used for soybean biodiesel production," *Data in Brief*, vol. 18, pp. 512–517, 2018.

[16] M. Hossain, N. Muntaha, L.K.M.O. Goni, M.S. Jamal, M.A. Gafur, D. Islam, A.N.M. Fakhruddin, "Triglyceride conversion of waste frying oil up to 98.46% using low concentration K^+/CaO Catalysts Derived from Eggshells." *ACS Omega*, vol. 6, no. 51, pp. 35679–35691, 2021.

[17] W. Purwaningrum, Y.F.C. Manurung, F. Fatma, A. Mara, "Modification of CaO from Quail Egg Shells with Sodium Dodecyl Sulfate through Extraction and Precipitation Method as Adsorbent for Methylene Blue Dyes." *Indonesian Journal of Fundamental and Applied Chemistry*, vol. 3, no. 5, pp. 155- 162, 2024.

[18] M. Mohamed, S. Yusup, M.A. Bustam, "Synthesis of CaO-based Sorbent from Biomass For CO_2 Capture in Series of Calcination- carbonation Cycle." *Procedia Engineering*, vol. 148, pp. 78–85, 2016.

[19] E. Aguila-Almanza, H. Hernandez-Cocoletzi, E. Rubio-Rosas, M. Calleja-Gonzales, H.R. Lim, K.S. Khoo, V. Singh, J.C. Maldonado-Montiel, P.L. Show, "Recuperation and

characterization of calcium carbonate from residual oyster and clamshells and their incorporation into a residential finish" *Chemosphere*, vol. 288, pp. 1–9, 2022.

[20] S. Mostofa, S.A. Jahan, B. Saha, N. Sharmin, S. Ahmed, "Kinetic and thermodynamic investigation on adsorption of lead onto apatite extracted From mixed Fish bone" *Environmental Nanotechnology, Monitoring & Management*, vol. 18, pp. 1–11, 2022.

[21] S. Khoo & H. Esmaeili, "Synthesis of CaO/Fe_3O_4 magnetic composite for the removal of Pb(II) and Co(II) from synthetic wastewater." *Journal of the Serbian Chemical Society*, vol. 83, no. 2, pp. 237–249, 2018.

[22] A.A. Bhat, F. Zafar, A.U. Mirza, A.H. Mondal, A. Kareem, Q.M.R. Haq, N. Nishat, "NiO nanoparticle doped-PVA-MF polymer nanocomposites: Preparation, Congo red dye adsorption and antibacterial activity," *Arabian Journal of Chemistry*, vol. 13, pp. 5724-5739, 2020.

[23] F. Riyanti, P.L. Hariani, Hasanudin, A. Rachmat, W. Purwaningrum, "Optimization Photodegradation of Methylene Blue Dye using Bentonite/PDA/Fe_3O_4@CuO Composite by Response Surface Methodology." *Bulletin of Chemical Reaction Engineering & Catalysis*, , vol. 19, no. 2, pp. 252-264, 2024.

[24] M. Abbas, S.R. Torati, S.A. Iqbal, C.G. Kim, "A novel and rapid approach for the synthesis of biocompatible and highly stable Fe3O4/SiO2 and Fe_3O_4/C core/shell nanocubes and nanorods." *New Journal of Chemistry*, vol. 41, pp. 2724–2734, 2017.

[25] X. Xie, J. Liao, X. Shao, Q. Li, Y. Lin, Y. "The Effect of shape on Cellular Uptake of Gold Nanoparticles in the forms of Stars Rods, and Triangles". *Scientific Reports*, vol. 7, pp. 3827–3836, 2017.

[26] X. Guo, F. Mao, W. Wang, W. Yang, Z. Bai, "Sulfhydryl-Modified Fe3O4@SiO2 Core/Shell Nanocomposite: Synthesis and Toxicity Assessment in Vitro." *ACS Applied Materials & Interfaces*, vol. 7, pp. 14983–14991, 2015.

[27] A. Nikmah, A. Taufiq, A. Hidayat, "Synthesis and Characterization of Fe_3O_4/SiO_2 nanocomposites" *IOP Conference Series: Earth and Environmental Science*, vol. 276, 2019.

[28] E.C. Peres, J.C. Slaviero, A.M. Cunha, A. Hosseini–Bandegharaei, G.L. Dotto, "Microwave synthesis of silica nanoparticles and its application for methylene blue adsorption." *Journal of Environmental Chemical Engineering*, vol. 6, pp. 649–659, 2018.

[29] P.L. Hariani, S. Salni, M. Said, & R. Farahdiba, R. "Core-shell $Fe_3O_4/SiO_2/TiO_2$ magnetic modified Ag for the photocatalytic degradation of Congo Red Dye and Antibacterial Activity," *Bulletin of Chemical Reaction Engineering and Catalysis*, vol. 18, no. 2, pp. 315–330, 2023.

[30] S. Tamjidi & H. Esmaeili, "Chemically Modified CaO/Fe_3O_4 Nanocomposite by Sodium Dodecyl Sulfate for Cr(III) Removal from Water." *Chemical Engineering and Technology*, vol. 42, no. 3, pp. 607–616, 2019.

[31] N.E. Augustus, A. Nimibofa, W. Donbebe, "Interpretation of Adsorption Thermodynamics and Kinetics." *Open Journal of Physical Chemistry*, vol. 10, pp. 166-182, 2020.

[32] S. Chatterjee, N. Guha, S. Krishnan, A.K. Singh, P. Mathur, & D.K. Rai, "Selective and Recyclable Congo Red Dye Adsorption by Spherical Fe_3O_4 Nanoparticles Functionalized with 1,2,4,5-Benzenetetracarboxylic Acid." *Scientific Reports*, vol. 10, no. 1, p. 111, 2020.

[33] E.C. Ijeamaka, O.C. Christian, O.O. Fabian, I.I. MaryJane, & K.T. Joseph, "Isotherm Studies of Adsorption of Cr (Vi) Ions onto Coconut Husk." *International Journal of Biochemistry, Biophysics & Molecular Biology*, vol. 3, no. 2, p. 38, 2018.

[34] Amrutha, J. Gautham, C.R. Girish, B. Prabhu, K. Mayer, "Multi-component Adsorption Isotherms: Review and Modeling Studies." *Environmental Processes*, vol. 10, p. 38, 2023.

[35] M.A. Al Ghouti, D.A. Da'ana, "Guidelines for the use and interpretation of adsorption isotherm models: A review." *Journal of Hazardous Materials*, Vol. 393, July 2020.

[36] R. Ragadhita, A. Bayu, D. Nandiyanto, & A.B.D. Nandiyanto, "How to calculate adsorption isotherms of particles using two-parameter monolayer adsorption models and equations." *Indonesian Journal of Science and Technology*, vol. 6, no. 1, pp. 205–234, 2021.

[37] B. Jayanna, V.M. Kulkarni O.D. Samuel, E. Linul "Sustainable biodiesel production from Oenothera lamarckiana oil using hybrid CaO@Fe3O4.SiO2 magnetic nanocatalyst: RSM- driven optimization." *Results in Engineering*, vol. 25, 2025.

[38] S. Shokri, N. Shariatifar, E. Molaee-Aghaee,

G.J. Khaniki, P. Sadighara, M.A. Faramarzi, "Synthesis and characterization of a novel magnetic chitosan–nickel ferrite nanocomposite for antibacterial and antioxidant properties," *Scientific Reports*, vol. 13, no. 1, 2023.

[39] P. Hu, L. Kang, T. Chang, F. Yang, H. Wang, Y. Zhang, J. Yang, K. she Wang, J. Du, Z. Yang, "High Saturation Magnetization Fe_3O_4 Nanoparticles Prepared by One-Step Reduction Method in Autoclave," *Journal of Alloys and Compounds*, vol. 728, pp. 88–92, 2017.

[40] P.L. Hariani, M. Said, A. Rachmat, S.P. Sari, "Hydroxyapatite-PEG/Fe_3O_4 Composite for Adsorption of Phenol from Aqueous Solution," *Polish Journal of Environmental Studies*, vol. 30, no. 2, pp. 1621–1629, 2021.

[41] Y. Wei, B. Han, X. Hu, Y. Lin, X. Wang, X. Deng, "Synthesis of Fe_3O_4 Nanoparticles and Their Magnetic Properties," *Procedia Engineering*, vol. 27, pp. 632–637, 2012.

[42] G.S. An, J.S. Han, J.R. Shin, D.H. Chae, J.U. Hur, H.Y. Park, Y.G. Jung, S.C. Choi, "In Situ Synthesis of Fe_3O_4@SiO_2 Core–Shell Nanoparticles via Surface Treatment," *Ceramics International*, vol. 44, no. 11, pp. 12233–12237, Aug. 2018.

[43] M.A. Ahmed, A.A. Mohamed, "A Systematic Review of Layered Double Hydroxide-Based Materials for Environmental Remediation of Heavy Metals and Dye Pollutants," *Inorganic Chemistry Communications*, vol. 148, Feb. 2023.

[44] T. Wang, M. Jiang, X. Yu, N. Niu, L. Chen, "Application of Lignin Adsorbent in Wastewater Treatment: A Review," *Separation and Purification Technology*, vol. 302, p. 122116, Dec. 2022.

[45] J. Wang, X. Guo, "Adsorption Kinetic Models: Physical Meanings, Applications, and Solving Methods," *Journal of Hazardous Materials*, vol. 390, p. 122156, , May 2020.

[46] H. Motaghi, P. Arabkhani, M. Parvinnia, A. Asfaram, "Simultaneous Adsorption of Cobalt Ions, Azo Dye, and Imidacloprid Pesticide on the Magnetic Chitosan/Activated Carbon@UiO-66 Bio-Nanocomposite: Optimization, Mechanisms, Regeneration, and Application," *Separation and Purification Technology*, vol. 284, p. 120258, Feb. 2022.

[47] A.M. Muliwa, O.A. Oyewo, A. Maity, "Recent Progress on the Removal of Aqueous Mercury by Carbon-Based Adsorbents: A Review," *Inorganic Chemistry Communications*, vol. 156, p. 111207, Oct. 2023.

[48] C. Wang, X. Liu, T. Yang, D. Sridhar, H. Algadi, B. B. Xu, Z. M. El-Bahy, H. Li, Y. Ma, T. Li, Z. Guo, "An Overview of Metal-Organic Frameworks and Their Magnetic Composites for the Removal of Pollutants," *Sep. Purif. Technol.*, vol. 320, p. 124144, Sep. 2023.

[49] X. Xing, N. S. Alharbi, X. Ren, C. Chen, "A Comprehensive Review on Emerging Natural and Tailored Materials for Chromium-Contaminated Water Treatment and Environmental Remediation," *Engineering*, vol. 10, no. 2, p. 107325, Apr. 2022.

[50] L.M. Calderon, C.B. Flores, V.P. Garcia, D.V. Yazigi, "Advances of Magnetic Nanohydrometallurgy Using Superparamagnetic Nanomaterials as Rare Earth Ions Adsorbents: A Grand Opportunity for Sustainable Rare Earth Recovery," *Separation and Purification Technology*., vol. 299, p. 121708, Oct. 2022.

[51] L. Ai, C. Zhang, Z. Chen, "Removal of Methylene Blue from Aqueous Solution by a Solvothermal-Synthesized Graphene/Magnetite Composite," *Journal of Hazardous Materials*, vol. 192, no. 3, pp. 1515–1524, 2011.

[52] S. Dhananasekaran, R. Palanivel, S. Pappu, "Adsorption of Methylene Blue, Bromophenol Blue, and Coomassie Brilliant Blue by α-Chitin Nanoparticles," *Journal of Advanced Research*, vol. 7, no. 1, pp. 113–124, 2016.

[53] R. Han, Y. Wang, P. Han, "Removal of Methylene Blue from Aqueous Solution by Chaff in Batch Mode," *Journal of Hazardous Materials*, vol. 137, no. 1, pp. 550–557, 2006.

[54] H. Chen, J. Zhao, G. Dai, "Silkworm Exuviae – A New Non-Conventional and Low-Cost Adsorbent for Removal of Methylene Blue from Aqueous Solutions," *Journal of Hazardous Materials*, vol. 186, no. 2–3, pp. 1320–1327, 2011.

[55] S.A. Umoren, U.J. Etim, A.U. Israel, "Adsorption of Methylene Blue from Industrial Effluent Using Poly (Vinyl Alcohol)," *Environmental Science*, vol. 4, no. 1, pp. 75–86, 2013.

[56] J. Ma, J. Zhang, D. Li, "Removal of Methylene Blue by Lava Adsorption and Catalysis Oxidation," *Environmental Technology*, vol. 31, no. 3, pp. 267–276, 2013.

[57] T.E. Rasilingwani, J.R. Gumbo, V. Masindi, S. Foteinis, "Removal of Congo Red Dye from Industrial Effluents Using Metal Oxide-Clay

Nanocomposites: Insight into Adsorption and Precipitation Mechanisms," *Water Resources and Industry*, vol. 31, p. 100253, 2024.

[58] M. Stjepanovic, N. Velic, A. Galic, I. Kosovic, T. Jakovljevic, M. Habuda-Stanic, "From Waste to Biosorbent: Removal of Congo Red from Water by Waste Wood Biomass," *Water*, vol. 13, no. 3, p. 279, 2021.

[59] M. Shakeel, S. Khizar, A. Atiq, S. Ali, "Equilibrium, Kinetic and Thermodynamic Studies for the Purification of Wastewater from Congo Red Using Simple and Low Cost Adsorbents," *Vietnam Journal of Chemistry*, vol. 61, no. 6, pp. 761–777, 2023.

[60] T.K. Roy, N.K. Mondal, "Biosorption of Congo Red from Aqueous Solution onto Burned Root of Eichhornia crassipes Biomass," *Applied Water Science*, vol. 7, no. 4, pp. 1841–1854, 2017.

[61] M.S. Hussain, R. Rehman, M. Imran, A. Dar, M. Akram, E.A. Al-Abbad, "Eco-Friendly Detoxification of Congo Red Dye from Water by Citric Acid Activated Bioadsorbents Consisting of Watermelon and Water Chestnuts Peels Collected from Indigenous Resources," *Adsorption Science & Technology*, vol. 2022, p. 9056288, 2022.

[62] D.O. Aderibigbe, A.A. Giwa, M.A. Oladipo, I.A. Bello, "Competitive Adsorption of Congo Red in Single and Binary Systems Using a Low-Cost Adsorbent," *Journal of Health and Pollution*, vol. 9, no. 31, 2021.

[63] M. A. Fawzy, M. Gomaa, "Low-Cost Biosorption of Methylene Blue and Congo Red from Single and Binary Systems Using Sargassum latifolium Biorefinery Waste/Wastepaper Xerogel: An Optimization and Modeling Study," *Journal of Applied Phycology* , vol. 33, no. 1, pp. 675–691, 2021.

[64] M. Ravikumar, P. King, "Application of Response Surface Optimization on Biosorption of Congo Red Dye onto Spathodea campanulata Leaves," *Desalination and Water Treatment*, vol. 182, pp. 342–350, 2020.

[65] Y.A.B. Neolaka, Y. Lawa, J.N. Naat, Y.K. Nubatonis, A.A.P. Riwu, "Studi Termodinamika Adsorpsi Pb (II) Menggunakan Adsorben Magnetik GO-Fe_3O_4 yang Disintesis dari Kayu Kusambi (*Schleichera oleosa*)," *Jurnal Saintek Lahan Kering*, vol. 2, no. 2, pp. 49–51, 2019.

[66] S. S. Alterary, A. AlKhamees, "Synthesis, Surface Modification, and Characterization of Fe_3O_4@SiO_2 Core@Shell Nanostructure," *Green Processing and Synthesis*, vol. 10, pp. 384–391, 2021.

[67] M. E. Khosroshahi, L. Ghazanfari, "Synthesis and Functionalization of SiO_2 Coated Fe_3O_4 Nanoparticles with Amine Groups Based on Self-Assembly," *Materials Science and Engineering: C*, pp. 1043–1049, 2012.